Sparsity-promoting photoacoustic imaging with source estimation

Shashin Sharan[1], Rajiv Kumar[1], Diego S. Dumani[2,3], Mathias Louboutin[4],
Rongrong Wang[5], Stanislav Emelianov[2,3] and Felix J. Herrmann[1,4]
[1] School of Earth and Atmospheric Sciences, Georgia Institute of Technology, Atlanta, GA, USA
[2] School of Electrical and Computer Engineering, Georgia Institute of Technology, Atlanta, GA, USA
[3] The Wallace H. Coulter Department of Biomedical Engineering,
Georgia Institute of Technology and Emory University, Atlanta, GA, USA
[4] School of Computational Science and Engineering, Georgia Institute of Technology, Atlanta, GA, USA
[5] Department of Computational Mathematics, Science and Engineering,
Michigan State University, Lansing, MI, USA

***Abstract*—Photoacoustics has emerged as a high-contrast imaging modality that provides optical absorption maps inside of tissues, therefore complementing morphological information of conventional ultrasound. The laser-generated photoacoustic waves are usually envelope-detected, thus disregarding the specific waveforms generated by each photoabsorber. Here we propose a sparsity-promoting image reconstruction method that allows the estimation of each photoabsorber's source-time function. Preliminary studies showed the ability to reconstruct the optical absorption map of an in silico vessel phantom. By using a sparsity-promoting imaging method, absorption maps and source-time functions can still be recovered even in situations where the number of transducers is decreased by a factor of six. Moreover, the recovery is able to attain higher resolution than conventional beamforming methods. Because our method recovers the source-time function of the absorbers, it could potentially also be used to distinguish different types of photoabsorbers, or the degree of aggregation of exogenous agents, under the assumption that these would generate different source-time functions at the moment of laser irradiation.**

***Index Terms*—sparsity promoting inversion, source-time function, wave equation, photoacoustic imaging**

I. Introduction

Applications of compressive sensing techniques in ultrasound and photoacoustic imaging have seen an increase in the last decade [1] - [3]. These techniques enable the estimation of waveform characteristics that are not readily available via conventional beamforming methods. Through the use of convex optimization techniques that promote sparsity, the frequency content of the ultrasound waves can be recovered beyond the Nyquist limit—i.e., from recordings of the induced wavefield that are well below the spatial Nyquist frequency.

In photoacoustic imaging, the optical absorption maps are usually created from envelope-detected waves [4]. While conventional beamforming techniques offer advantages, including real-time image reconstruction, they often disregard the frequency content of the measured waves. Additionally, the available frequency content is always band-limited by the receiving transducers. In ultrasound imaging, several studies have shown that the frequency content of raw pressure waves can provide information of tissue composition, in applications such as ophthalmic, rectal, and intravascular imaging [5] - [8]. Similar concepts have been explored in photoacoustics [9], denoting that there is a potential use of the photoacoustic wave frequency content. The study of RF photoacoustic techniques could further enhance the functional and molecular imaging capabilities of this modality [10].

Recently, a sparsity-promoting algorithm for the estimation of full-wave source-time functions was developed as a method to localize microseismic events for geological exploration [11]. In photoacoustic imaging, the localization of strong photoabsorbers in tissue represents an analog problem albeit that in microseismic the source firing times differ for each source and are not known. The fact that these source-time functions are unknown make the microseismic problem more challenging because it leads to a large non-trivial nullspace—i.e., there exist so-called non-radiating sources that correspond to sources that do not contribute to wavefield measured at the receivers. Conventional photoacoustic imaging overcomes this problem by assuming the absorbers to fire synchronously. As a result, high-fidelity images can be obtained by time reversal, followed by extraction of the back propagated wavefield at $t = 0$. While this method has proven to be highly succesful, it relies on dense sampling and does not provide information on the source-time function of the different absorbers. Our sparsity-promoting method on the other hand, is able to handle the large null space and as such can handle sparse samplings of the wavefield while providing information on the source-time functions. The latter could potentially be used for tissue and contrast agent characterization.

Our contribution is organized as follows. First, we provide an overview of our methodology including statement of the problem, solution by linearized Bregman, and acceleration with a dual formulation. Next, we demonstrate our method on a phantom in a constant velocity model, yielding an estimate for the phantom and the source-time function. We follow this result by a series of experiments where the number of transducers (receivers) is reduced significantly. We compare

our results to those obtained with time reversal. We conclude by showing an example with a background velocity model that varies strongly.

II. Methodology

Contrary to conventional time-reversal methods, our unknown is a wavefield across the domain of interest and a function of time without making assumptions on the source waveform. Since the sources are of short duration firing at approximately the same time, we restrict the unknown wave by putting its entries to zero after a user specified number of time samples. Since the number of absorbers is small, we assume sparsity in space and finite energy along time. The latter makes sense because the photoabsorbers emit a finite amount of energy. To image the wavefield induced by these sparsely distributed absorbers, we solve

$$\min_{\mathbf{Q}\in\mathcal{T}_\tau} \quad \|\mathbf{Q}\|_{2,1} \quad \text{s.t.} \quad \|\mathcal{F}[\mathbf{m}](\mathbf{Q})-\mathbf{d}\|_2 \leq \epsilon, \tag{1}$$

with $\mathbf{Q} \in \mathbb{R}^{n_x \times n_t}$ being the unknown source wavefield, which we restrict to a user defined duration τ—i.e, $\mathcal{T}_\tau = \{\mathbf{Q} \,|\, \mathbf{Q}(\cdot, t) = 0, t > \tau\}$. The source wavefield in (1) consists of n_x grid points in space and n_t time samples. The matrix $\mathcal{F}[\mathbf{m}]$ represents the acoustic forward modeling operator parametrized by $\mathbf{m}$ the discretized squares slowness. Slowness is defined as the inverse of the acoustic wave speed.

Solving (1) corresponds to minimizing the $\ell_{2,1}$-norm of the unknown source wavefield $\mathbf{Q}$ while fitting the observed data $\mathbf{d}$ within ϵ, which depends on the noise level. After solving for $\mathbf{Q}$, we detect the location of sources as outliers in the intensity plot $\mathbf{I}(\mathbf{x}) = \text{vec}^{-1}(\mathbf{Q}(\mathbf{x}, t = t_0))$, where $\text{vec}^{-1}(\cdot)$ reshapes the vector into its original matrix form and t_0 is the firing time (typically the maximum of the source-time function). We finally estimate the associated source-time functions as the temporal variation extracted from the estimated source wavefield $\mathbf{Q}$ at the detected source locations.

A. Linearized Bregman Algorithm

Equation (1) is similar to the classic basis pursuit denoising (BPDN) problem [12] involving a sparsity-promoting objective and a data constraint. With the recent successful application of the linearized Bregman algorithm [13], [14] to seismic imaging [15] and microseismic source estimation problems [11], we use this method to solve BPDN via a relaxed form that is strongly convex. Following [11], we minimize

$$\min_{\mathbf{Q}\in\mathcal{T}_\tau} \quad \|\mathbf{Q}\|_{2,1}+\frac{1}{2\mu}\|\mathbf{Q}\|_F^2 \quad \text{s.t.} \quad \|\mathcal{F}[\mathbf{m}](\mathbf{Q})-\mathbf{d}\|_2 \leq \epsilon, \tag{2}$$

where μ is a tradeoff parameter between the sparsity $\ell_{2,1}$-norm and the Frobenius norm $\|.\|_F$. As $\mu \uparrow \inf$, (2) becomes equivalent to (1). Therefore, for large enough μ, the solution of (2) approaches the solution of (1), which in principle should give us a high resolution photoabsorber image. Unfortunately, for increasing values of μ, the linearized Bregman algorithm requires more iterations making this method prohibitively expensive because each iteration requires one forward and one time-reversed simulation [11]. We denote the adjoint by the superscript $^\top$.

B. Acceleration using a dual formulation

Reference [16] showed that solving the original problem (2) through linearized Bregman iterations is equivalent to solving its dual formulation through gradient descent steps. Therefore, we use gradient descent acceleration method such as spectral projected gradient (SPG) method to accelerate the convergence of the linearized Bregman algorithm. To arrive at this accelerated algorithm, we derive the Fenchel's dual of problem (2) yielding

$$\min_{\mathbf{y}} \quad f(\mathbf{y}) = -\left\{\Psi(\mathbf{y}) - \epsilon\|\mathbf{y}\|_2\right\}, \tag{3}$$

where $\mathbf{y}$ is the dual variable and

$$\Psi(\mathbf{y}) = \min_{\mathbf{Q}\in\mathcal{T}_\tau} \|\mathbf{Q}\|_{2,1} + \frac{1}{2\mu}\|\mathbf{Q}\|_F^2 + \mathbf{y}^\top\big(\mathcal{F}[\mathbf{m}](\mathbf{Q})-\mathbf{d}\big), \tag{4}$$

is a value function of the dual variable $\mathbf{y}$. The dual objective function gives the minima of the objective function defined in (3) as a function of the dual variable $\mathbf{y}$. We derive the gradient $\nabla f(\mathbf{y})$ of the dual objective function $f(\mathbf{y})$ as

$$\nabla f(\mathbf{y}) = -\left\{\nabla\Psi(\mathbf{y}) - \epsilon\mathbf{y}/\|\mathbf{y}\|_2\right\}, \tag{5}$$

where

$$\nabla\Psi(\mathbf{y}) = \mathbf{d} - \mathcal{F}[\mathbf{m}]\big(\text{Prox}_{\mu\ell_{2,1}}(\mu\mathcal{F}[\mathbf{m}]^\top(\mathbf{y})\big) \tag{6}$$

is the gradient of the value function $\Psi(\mathbf{y})$. The proximal operator in this expression is equivalent to a thresholding operation and its action on a matrix $\mathbf{C}$ is defined as:

$$\text{Prox}_{\mu\ell_{2,1}}(\mathbf{C}) := \arg\min_{\mathbf{B}} \|\mathbf{B}\|_{2,1} + \frac{1}{2\mu}\|\mathbf{C}-\mathbf{B}\|_F^2 \,. \tag{7}$$

The main steps of the linearized Bregman with acceleration are summarized in Algorithm (1).

Algorithm 1 Acceleration with SPG.

1. Data $\mathbf{d}$, slowness square $\mathbf{m}$, number of iterations l `//Input`
2. Initialize dual variable $\mathbf{y} = 10^{-3}\mathbf{d}$
3. $\hat{\mathbf{y}} = \text{SPG}(f(\mathbf{y}), \nabla f(\mathbf{y}), \mathbf{y}, l)$ `//Dual solution`
4. $\mathbf{Q} = \text{Prox}_{\mu\ell_{2,1}}(\mu\mathcal{F}[\mathbf{m}]^\top(\mathbf{y}))$ `//Primal solution`

III. Experiments

To demonstrate our ability to jointly image and estimate the source-time function, we performed simulation experiments in acoustic medium using JUDI [17] and Devito [18] - [19], a high performance finite difference partial differential equation solver and the k-Wave MATLAB toolbox [20]. To avoid problems with the boundaries of the domain, we use derivatives of the Gaussian as the source-time function. In this way, we avoid low frequencies to enter into the solution so we can limit the size of the absorbing boundary layer. By casting photoacoustic imaging as a sparsity-promoting imaging problem, we are able to estimate the source-time function from poorly sampled wavefields. To illustrate this, we first carry

out an imaging experiment in a constant velocity model that is densely sampled and show that we can indeed estimate the source-time function. Next, we compare images obtained with the proposed method and with the back-propagation method for increasingly poor sampling, followed by an example in a strongly heterogeneous medium. For all experiments, we use Devito to generate data. For the time reversal method, we generate data using k-Wave MATLAB toolbox, which has a broader frequency content in comparison to the data we use.

A. *Image and source-function recovery from dense data*

Fig. 1a shows the actual location of photoabsorbers (solid white color) and white color dots indicate the transducers. The background is constant with an acoustic wave velocity of $1500\,\mathrm{m/s}$. We obtain a high resolution image in Fig. 1b with the proposed method. We are also able to reconstruct the source-time functions (red color plots in Figs. 1c and 1d), which is close to the true source-time function (cf. Figs. 1c and 1d).

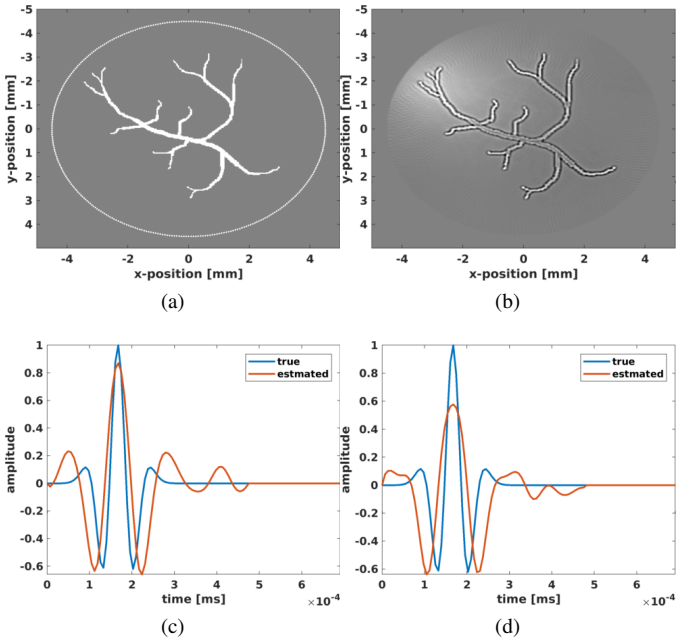

Fig. 1: (a) Data acquisition with locations of the photoabsorbers denoted by the solid white color phantom and transducers by white color dots (b) Image reconstructed from fully sampled data using our proposed method. (c) and (d) show a source-time function comparison for two locations.

B. *Image recovery from subsampled data*

Figs. 2a and 2b contain photoabsorber images we reconstructed with the proposed method from transducers sampled at every two degrees and every six degrees. Although we see some background noise when the transducer sampling becomes poor, the proposed method is still able to get a reasonable high resolution image in comparison to the image obtained using the back-propagation method of the k-wave toolbox (cf. Figs. 2c and 2d). As the sparsity of transducers increases, we observe blurring of the images obtained with time reversal.

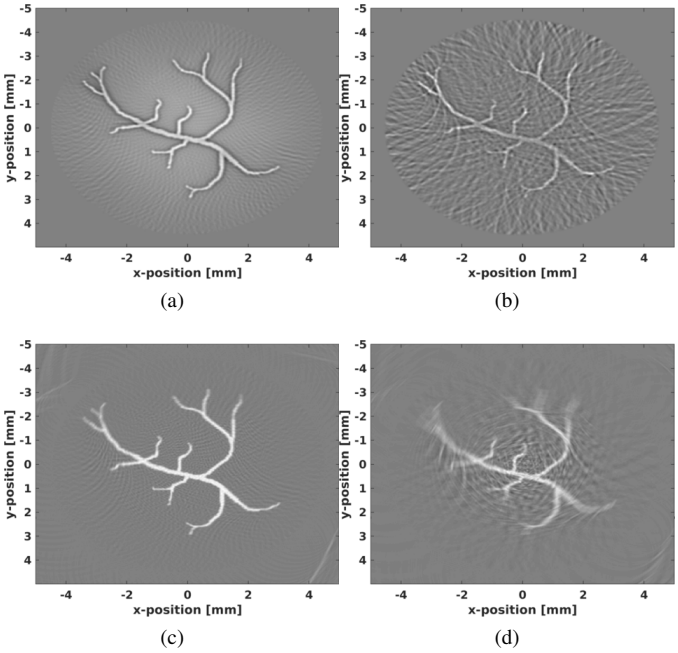

Fig. 2: Receiver sparsity experiment: Reconstructed image with transducers at every (a) 2 degrees and (b) 6 degrees using proposed method. Image with transducers at every (c) 2 degrees and (d) 6 degrees using k-wave toolbox

C. *Image recovery in strongly heterogenous media*

In this experiment, we show imaging results and source-time reconstruction using a kinematically correct smooth velocity model and data simulated with the hard model in Fig. 3a with a background wave speed of $1500\,\mathrm{m/s}$ and two lobes with $1575\,\mathrm{m/s}$ and $1650\,\mathrm{m/s}$, repectively. We obtain the image plotted in Fig. 3c with a smooth velocity model with the proposed method. Although, the image obtained with our method is somewhat lower in resolution in comparison to the images obtained with time reversal (Fig. 3d). This is because of the higher frequency content of the k-wave data. Still, the proposed method gives a good estimate for the source-time function when using the original hard model and the smoothed model (cf. red and yellow lines in Fig. 3b). The amplitudes of the estimated source-time functions can be corrected with a debiasing step.

IV. Discussion and Conclusions

Photoacoustic imaging is a powerful method, which in part derives its performance by more or less complete elimination of the source-time function from the inversion procedure. While this obviously has the advantage of reducing the size of the unknowns, it does not allow us to study the frequency-dependence of the absorption mechanism locally. In addition, imaging by a single time-reversed imaging step relies on dense sampling, which strains the acquisition system.

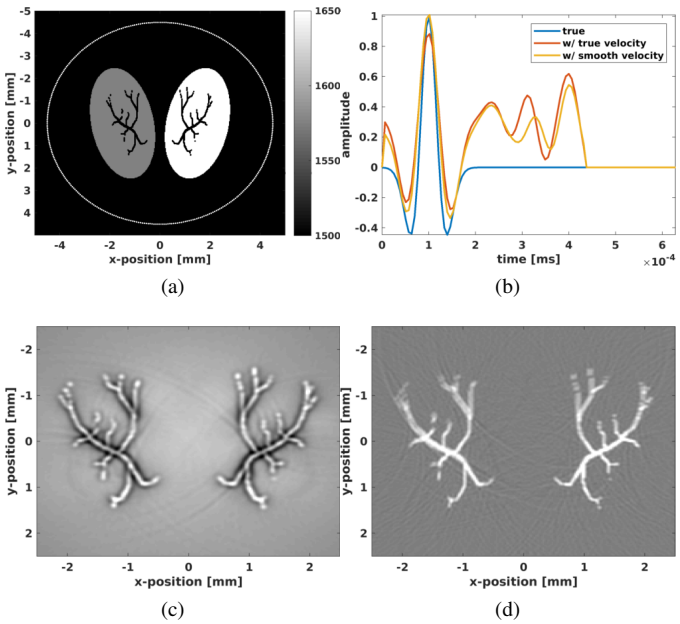

Fig. 3: Heterogeneous medium experiment: (a) Heterogeneous medium with hard discontinuities. (b) Source-time functions true (blue) and estimated with the true (red) and smoothed velocity (orange). Reconstructed photoabsorber image (zoomed) using smooth velocity with (c) proposed method and with (d) k-wave.

Aside from being able to obtain more information on the source mechanism, our formulation is also robust with respect to poor sampling while it allows for media with strongly varying velocities. In the latter case, we only need access to a smooth velocity model that is kinematically correct. We achieve robustness with respect to the sampling by virtue of promoting structure on the image. For now, we only imposed sparsity, which may not be reasonable when photoabsorbers form objects that exhibit spatial continuity such as the used phantom. Still, our method is capable of producing images for poor sampling because the subsampling artifacts are not sparse, which is paramount to the success of compressive sensing. Despite the less than ideal assumptions—i.e., the sources are not sparsely distributed Dirac deltas, our approach produces reasonable results while opening a perspective of being able to estimate the frequency-dependence of the sources, which may allow us to distinguish between different types of photoabsorbers.

ACKNOWLEDGMENT

We would like to acknowledge the support from the SINBAD II project and support of the member organizations of the SINBAD Consortium. We would also like to acknowledge Georgia Research Alliance.

REFERENCES

[1] H. Liebgott, A. Basarab, D. Kouame, O. Bernard, and D. Friboulet, "Compressive sensing in medical ultrasound," IEEE Int. Ultra Sym., pp. 1–6, 2012.

[2] J. Provost, and F. Lesage, "The application of compressed sensing for photo-acoustic tomography," IEEE T. Med Imaging, 28(4),pp. 1–6, 2009.

[3] P. Kruizinga, P. van der Meulen, A. Fedjajevs, F. Mastik, G. Springeling, N. de Jong, J.G. Bosch and G. Leus, "Compressive 3D ultrasound imaging using a single sensor," Science advances, 3(12), e1701423., 2017.

[4] S. Park, A. B. Karpiouk, S. R. Aglyamov, and S. Y. Emelianov, "Adaptive beamforming for photoacoustic imaging using linear array transducer," IEEE Int. Ultra Sym., pp. 1088–1091, Nov 2008.

[5] F.L. Lizzi, M. Greenebaum, E.J. Feleppa, M. Elbaum, and D.J. Coleman, " Theoretical framework for spectrum analysis in ultrasonic tissue characterization," J Acoust. Soc. Am., 73(4), pp. 1366–1373, 1983.

[6] E.J. Feleppa, A. Kalisz, J.B. Sokil-Melgar, F.L. Lizzi, T. Liu, A.L. Rosado, and V.E. Reuter, "Typing of prostate tissue by ultrasonic spectrum analysis," IEEE T. Ultrason. Ferr., 43(4), pp. 609–619, 1996.

[7] F.L. Lizzi, "Ultrasonic scatterer-property images of the eye and prostate," In IEEE Ultrasonics Symposium Proceedings., Vol. 2, pp. 1109-1117, 1997.

[8] M. P. Moore, T. Spencer, D.M. Salter, P.P. Kearney, T. R. D. Shaw, I.R. Starkey, et al., "Characterisation of coronary atherosclerotic morphology by spectral analysis of radiofrequency signal: in vitro intravascular ultrasound study with histological and radiological validation," Heart, 79(5), pp. 459-467, 1998.

[9] R. E. Kumon, C. X. Deng, and X. Wang, "Frequency-domain analysis of photoacoustic imaging data from prostate adenocarcinoma tumors in a murine model," Ultrasound in medicine and biology, 37(5), pp. 834-839, 2011.

[10] S. Y. Emelianov, Pai-Chi Li, and Matthew O'Donnell, "Photoacoustics for molecular imaging and therapy," Physics Today, 62(5):34–39, 2009. doi: 10.1063/1.3141939

[11] S. Sharan, R. Wang, and F.J. Herrmann, "Fast sparsity-promoting microseismic source estimation," Geophys. J. Int., in press.

[12] S.S. Chen, D.L. Donoho, and M.A. Saunders, "Atomic Decomposition by Basis Pursuit," SIAM J. Sci. Comput., 20(1), pp. 33-61, 1998.

[13] W. Yin, S. Osher, D. Goldfarb, and J. Darbon "Bregman Iterative Algorithms for ℓ_1-minimization with Applications to Compressed Sensing," SIAM J. Imaging. Sci., 1(1), pp. 143–168, 2008.

[14] D.A. Lorenz, F. Schöpfer, and S. Wenger, "The Linearized Bregman Method via Split Feasibility Problems: Analysis and Generalizations," SIAM J. Imaging Sci., 7(2), pp. 1237–1262, 2014.

[15] P.A. Witte, M. Louboutin, F. Luporini, G.J. Gorman, and F.J. Herrmann, "Compressive least-squares migration with on-the-fly Fourier transforms," unpublished.

[16] W. Yin, "Analysis and Generalizations of the Linearized Bregman Method," SIAM J. Imaging. Sci., 3(4), pp. 856–877, 2010.

[17] P. A. Witte, M. Louboutin, N. Kukreja, F. Luporini, M. Lange, G.J. Gorman, et al., "A large-scale framework for symbolic implementations of seismic inversion algorithms in Julia," unpublished, 2018.

[18] M. Louboutin, M. Lange, F. Luporini, N. Kukreja, P. A. Witte, F.J. Herrmann, et al., "Devito: an embedded domain-specific language for finite differences and geophysical exploration," CoRR, abs/1808.01995, 2018. https://github.com/opesci/devito

[19] F. Luporini, M. Lange, M. Louboutin, N. Kukreja, J. Hückelheim, C. Yount, et al., "Architecture and performance of Devito, a system for automated stencil computation," CoRR, abs/1807.03032, 2018.

[20] B. E. Treeby, and B. T. Cox, "k-Wave: MATLAB toolbox for the simulation and reconstruction of photoacoustic wave-fields," J. Biomed. Opt., 15(2), pp. 021314, 2010. http://www.k-wave.org/